Finite deformation elasto-plastic modelling using an adaptive meshless method.

Z. Ullah (corresponding author)
School of Engineering and Computing Sciences,
Durham University,
Durham, DH1 3LE, UK
zahur.ullah@dur.ac.uk

C.E. Augarde
School of Engineering and Computing Sciences,
Durham University,
Durham, DH1 3LE, UK
charles.augarde@dur.ac.uk

Abstract

Problems including both material and geometric nonlinearities are of practical engineering importance in many applications. Efficient computational modelling of these problems with minimum computer resources remains challenging. Often these problems are modelled with the finite element method (FEM) with adaptive analysis, in which an error estimation procedure automatically determines regions for coarse and fine discretization. Meshless methods offer the attractive possibility of simpler adaptive procedures involving no remeshing, simply insertion or deletion of nodes. However, as meshless methods are computationally more expensive than the FEM, the use of the minimum possible number and proper distribution of nodes are important issues. In this study an adaptive meshless approach for nonlinear solid mechanics is developed based on the element free Galerkin method. An existing error estimation procedure for linear elasto-static problems, is extended here for nonlinear problems including finite deformation and elasto-plasticity, and a new adaptive procedure is described and demonstrated.

Keywords: meshless, meshfree, EFG, adaptive analysis, error estimation.

1 INTRODUCTION

The finite element method (FEM) is the most prominent numerical tool for the solution of linear and non-linear boundary value problems in computational mechanics. Robust FEM commercial codes are available, and are widely used for the solution of practical engineering problems. In spite of these positive points, the FEM can struggle, particularly when considering nonlinear problems where issues such as high pre-processing time, low accuracy of stresses and complexity of adaptive procedures become important. It is also not ideal for certain classes of problems, e.g. crack growth, moving boundaries and large deformation problems [1] and various refinements are necessary, XFEM for fracture for instance. Indeed in this area major advances have been made [2–4]. With mesh-based numerical methods, one cannot avoid the issues of element distortion and the need for remeshing in finite deformation problems (which also brings the difficulty of projection of information from one mesh to another). With these issues in mind, meshless methods are an attractive alternative as only a set of nodes is required for the problem discretization and most of the main drawbacks of mesh-based methods disappear. In this paper we present details of a meshless modelling procedure for finite deformation elasto-plasticity which brings together a number of ideas and features including max-ent, error estimation and adaptive refinement into a single model. The modelling is restricted here to continuum problems and we do not present results or solutions for fracture modelling, although we do note the links to the literature in this area in the text.

A number of different meshless methods have been developed for solid mechanics since 1990 and detailed reviews can be found in [5–7]. The element free Galerkin method (EFGM) is one of the most widely used, in which moving least squares (MLS) approximations are used as test and trial functions, background cells are employed for numerical integration in the weak form and essential boundary conditions are enforced using Lagrange multipliers. The EFGM has been used to model a variety of physics, e.g. $2D$ linear elasticity [8–10], static and dynamic fracture mechanics [11, 12], plate and shell analysis [13–15], vibration [7, 16, 17], electromagnetics [18], heat transfer [8, 19–21], metal forming [22, 23], biomechanics [24, 25] and geomechanics [26]. While the EFGM is superior to the FEM in terms of accuracy and convergence, and there are no issues of volumetric locking [27], MLS shape functions are computationally more expensive and complicate the imposition of essential boundary conditions. The use of Lagrange multipliers for the latter also increases the dimension of the final system of equations and the stiffness matrix is no longer positive definite [28]. Other examples of meshfree approaches applied to cracking problems can be found in [29–31]. A related meshfree method is the finite point method which also uses MLS techniques but adds stabilization and was developed first for fluid mechanics [32] but later was applied to solid mechanics [33]. Smoothed finite element methods (SFEMs) are often cited as competitors to meshless methods such as the EFGM. In SFEMs a modified or constructed strain field is used, which involves only the shape functions. The Galerkin weak form is also changed to get stability and convergence. The SFEM was first proposed in [34] for linear elastic problems. Based on its strain smoothing formulation it is divided into cell based (CS-FEM) in [35], n-sided polygonal

(nSFEM) [36], node based (NS-FEM) [37], edge based (ES-FEM) for 2D [7], and face based (FS-FEM) for 3D [38]. Its properties, convergence and accuracy are discussed in [39] and it has been used in adaptive analysis [40].

Returning to the EFGM, a recent and welcome advance in shape function formulations for meshless methods have been those based on maximum entropy (max-ent) concepts. These lead to formulations in which imposition of essential boundary conditions is as straightforward as in the FEM. Sukumar [41] describes the link between concepts of informational entropy [42], maximum entropy [43, 44] and global approximations to a function. Non-local and non-interpolating characteristics of these shape functions are highlighted in [45] where the (more useful) local max-ent formulation is introduced and incorporated into meshless modelling of linear and non-linear elasticity. Compact support shape functions are derived using Gaussian weight functions (or priors) in [45], work which is extended in [46] for any weight function (or generalized prior). First-order consistent max-ent shape functions [46] are then extended to second order in [47] and max-ent is used in [48] for the automatic calculation of the nodal domain of influence within a meshless method. Other recent examples of the use of max-ent in meshless methods can be found in [49–52]. Another option which is not considered here is the use of so-called interpolatory MLS, which satisfies the Kronecker delta property and is used for imposition of the essential boundary condition in the EFGM in [53] and also in other meshless methods [54]. In these approaches a singular weight function is used. However careful choices are necessary for the arrangements of the domains of influence of nodes otherwise the methods acncan become unstable [55].

It is clearly recognized in FE modelling that adaptive procedures based on robust error estimates are necessary to remove user-bias and to automate analyses, and mature procedures are now available, many based on recovery type measures such as the famous Zienkiewicz-Zhu approach. Error estimation procedures based on constitutive relations for linear FE problems are also well developed, e.g. [56–58]. The idea here is to calculate an admissible displacement and stress field from the finite element solution which satisfies the kinematic and equilibrium equations but will not satisfy the constitutive relation, from which the error measure is drawn. These are also extended to nonlinear problems in [59–62]. Residual based error estimation methods for FEs were first proposed in [63] which are further divided into explicit and implicit depending on the use of the residual. Details of explicit methods can be found in many references, e.g. [64, 65] and the implicit in [66–68]. An interesting avenue of research in error estimation can also be found in the works of Larsson & Runesson [69].

Error estimation and adaptivity have yet to become widely used in meshless methods partly because of the current lack of a firm mathematical basis for error estimation as has been developed for FEs. However there is evidence of a strong interest as indicated in the following. Chung and Belytschko [70] describe possibly the first error estimator for the EFGM using the difference between raw EFGM results and projected stresses from the same nodal distribution but with reduced domains of influence. In [71] error estimation and adaptivity

is performed using stress gradients, thus requiring second derivatives of the meshless shape functions. In [72] a computationally efficient method for error estimation based on tessellation is proposed for the EFGM, i.e. error at a Gauss point is calculated as the difference between the EFGM stress or strain and that calculated at the nearest node. A slight change is made in [73] where comparison is instead made with a field calculated using a first order Taylor series expansion with a four quadrant criterion, and the two approaches are compared by the same authors in [74]. [75] describes an error estimate for the EFGM based on a Taylor series with a higher order derivative and a structured grid is used instead of a cloud of points, which makes the implementation very straightforward. Error estimation based on the gradient of strain energy density is proposed in [76] and an adaptive analysis for EFGM is proposed in [77] based on background cells, error being estimated based on two different integration orders and a refinement algorithm based on local Delaunay triangulation is also proposed. In [78], the approach from [70] is used for error estimation and adaptive analysis in crack propagation problems. A Zienkiewicz-Zhu type recovery type error estimator is proposed in [79]; two methods are used for stress recovery including that due to Chung & Belytschko [70] with the discrete MLS over a stationary least square fitting and it is found that the approach of [70] is more effective, and is used further for adaptive analysis in [80].

The survey of the current literature reveals that to date, for continuous problems (i.e. excluding fracture) adaptive meshless methods have been limited in their use to elasto-static problems with infinitesimal strains. In this paper we incorporate a new adaptive procedure into the max-ent EFGM for material and geometrically nonlinear problems in solid mechanics including a robust means of transferring data between discretizations. The paper is structured as follows. In §2.1 the EFGM and max-ent shape functions are briefly reviewed. The formulation adopted for finite deformation and elasto-plasticity are then given in §2.2. Error estimation and adaptive procedures for the EFGM are discussed in §2.3, including an error estimation formulation for linear problems which is extended in §2.3.2 to nonlinear problems. The meshless refinement strategy is explained in §2.3.3, followed by the means of transfer of path dependent variables from one discretization to the next. Numerical examples follow in §3 to show the performance of the current approach.

2 MODEL COMPONENTS

2.1 The Element Free Galerkin method with max-ent shape functions

The element free Galerkin method is developed as follows, considering for clarity a 2D elasto-static problem in $[x\ ,\ y]^T$ (extension to 3D is trivial), in domain Ω bounded by Γ. The equilibrium equations at a material point $\mathbf{x}$ are written as

$$\boldsymbol{\nabla}^T \cdot \boldsymbol{\sigma} + \mathbf{b} = 0 \qquad \text{in } \Omega, \tag{1}$$

subject to boundary conditions of $\boldsymbol{\sigma} \cdot \mathbf{n} = \bar{\mathbf{t}}$ on Γ_t and $\mathbf{u} = \overline{\mathbf{u}}$ on Γ_u where $\Gamma_u \bigcup \Gamma_t \equiv \Gamma$. Here $\boldsymbol{\sigma}$ is the Cauchy stress vector, $\bar{\mathbf{t}}$ is a vector of prescribed tractions on traction boundaries Γ_t, $\overline{\mathbf{u}}$ is a vector of prescribed displacements on essential boundaries Γ_u, $\mathbf{n}$ is unit normal, $\mathbf{b}$ is body force vector and the differential operator

$$\boldsymbol{\nabla} = \begin{Bmatrix} \frac{\partial}{\partial x} & 0 \\ 0 & \frac{\partial}{\partial y} \\ \frac{\partial}{\partial y} & \frac{\partial}{\partial x} \end{Bmatrix}. \tag{2}$$

The weak form of Equation 1 is written as

$$\int_{\Omega} \mathbf{V}^T \cdot \left(\boldsymbol{\nabla}^T \cdot \boldsymbol{\sigma} + \mathbf{b} \right) d\Omega = 0. \tag{3}$$

where $\mathbf{V}$ is a vector of test functions, which are chosen to be the same as the shape functions in the EFGM. Equation 3 can be discretized using an approximation to the displacement field in Ω

$$u^h(\mathbf{x}) = \boldsymbol{\phi}(\mathbf{x})^T \hat{\mathbf{u}}(\mathbf{x}), \tag{4}$$

where $\boldsymbol{\phi}$ is a $n \times 1$ vector of shape function values, $\hat{\mathbf{u}}$ is a $n \times 1$ vector of nodal parameters (or fictitious nodal values) for the n nodes in support at the point of interest $\mathbf{x}$. Combining Equations 3 & 4 and after further standard steps the final discrete system of linear equations is written as

$$\mathbf{K}\mathbf{u} = \mathbf{f}, \tag{5}$$

where

$$\mathbf{K}_{ij} = \int_{\Omega} \mathbf{B}_i^T \mathbf{D} \mathbf{B}_j d\Omega, \tag{6}$$

$$\mathbf{f}_i = \int_{\Gamma_t} \boldsymbol{\phi}_i \bar{\mathbf{t}} \ d\Gamma + \int_{\Omega} \boldsymbol{\phi}_i \mathbf{b} \ d\Omega, \tag{7}$$

$$\mathbf{B}_i = \begin{bmatrix} \frac{\partial \phi_i}{\partial x} & 0 \\ 0 & \frac{\partial \phi_i}{\partial y} \\ \frac{\partial \phi_i}{\partial y} & \frac{\partial \phi_i}{\partial x} \end{bmatrix}, \tag{8}$$

$$\mathbf{D} = \frac{\overline{E}}{1 - \overline{\nu}^2} \begin{bmatrix} 1 & \overline{\nu} & 0 \\ \overline{\nu} & 1 & 0 \\ 0 & 0 & \frac{1-\overline{\nu}}{2} \end{bmatrix}, \tag{9}$$

with

$$\overline{E} = \begin{cases} E & \text{for plane stress,} \\ \frac{E}{1-\nu^2} & \text{for plane strain,} \end{cases} \tag{10a}$$

$$\overline{\nu} = \begin{cases} \nu & \text{for plane stress,} \\ \frac{\nu}{1-\nu} & \text{for plane strain,} \end{cases} \tag{10b}$$

here ν is the Poisson's ratio and E is the modulus of elasticity.

Max-ent shape functions are used for the approximation of the field variable (displacement) in this study. These shape functions are strictly positive and possess a weak Kronecker delta property at the boundaries, which facilitates the direct imposition of the essential boundary conditions. We now briefly summarize their derivation.

The max-ent concept comes from information theory [42] where a measure of the amount of information or uncertainty of a finite scheme is termed information entropy and is given as

$$H(p_1, ..., p_n) = -\sum_{i=1}^{N} p_i \log p_i, \tag{11}$$

where $p_1, ..., p_n$ are n probabilities of n mutually independent events. The most likely probability distribution is obtained by using Jaynes' principle of max-ent [43], i.e. maximising Equation 11 subject to constraints $\sum_{i=1}^{n} p_i = 1$ and $\sum_{i=1}^{n} p_i g_r(x_i) = \langle g_r(x) \rangle$, where $\langle g_r(x) \rangle$ is the expectation of a function $g_r(x)$. The max-ent approach can be used to derive shape functions by seeing an analogy between the probabilities above and the shape function values themselves. A useful local shape function formulation can be obtained [46] by incorporating prior distributions w_i which can be regarded as weight functions that provide compact support, and then maximising the following

$$H(\phi, w) = -\sum_{i=1}^{n} \phi_i \log\left(\frac{\phi_i}{w_i}\right), \tag{12}$$

again subject to the standard constant and linearly reproducing constraints

$$\sum_{i=1}^{n} \phi_i = 1, \quad \sum_{i=1}^{n} \phi_i x_i = x, \quad \sum_{i=1}^{n} \phi_i y_i = y. \tag{13}$$

Shape functions can be derived as

$$\phi_i = \frac{Z_i}{Z} \tag{14}$$

where

$$Z_i = w_i e^{-\lambda_1 \widetilde{x}_i - \lambda_2 \widetilde{y}_i}, \qquad \& \qquad Z = \sum_{j=1}^{n} Z_j, \tag{15}$$

in which w_i is the weight function associated with node i, evaluated at point $\mathbf{x} = \{x, y\}^T$, $\widetilde{x_i} = x_i - x$ and $\widetilde{y_i} = y_i - y$ are shifted coordinates. n is the number of nodes in support at $\mathbf{x}$ and λ_1 and λ_2 are Lagrange multipliers which can be found from

$$\{\lambda_1, \lambda_2\} = \text{argmin } F(\{\lambda_1, \lambda_2\}), \qquad \text{where } F(\{\lambda_1, \lambda_2\}) = \log(Z). \tag{16}$$

F is a convex function and Newton's method is used to solve Equation (16) to find the Lagrange multipliers which can then be used in the expressions for the shape functions.

The weight function is an important part of the max-ent shape function formulation. In this study a cubic spline weight function is used. In the one-dimensional case the cubic spline weight function is written as

$$w\left(x-x_i\right)=w\left(r\right)=\begin{cases}\frac{2}{3}-4r^2+4r^3 & \text{for } r\leq\frac{1}{2},\\ \frac{4}{3}-4r+4r^2-\frac{4}{3}r^3 & \text{for } \frac{1}{2}<r\leq 1,\\ 0 & \text{for } r>1,\end{cases} \tag{17}$$

Here, $r=\frac{d_i}{d_{mi}}$ is the normalized distance, where $d_i=\|x-x_i\|$ is the distance between node i and point of interest (in 1D) x and d_{mi} is the domain of influence of a node and is written as $d_{mi}=d_{max}c_i$ where d_{max} is a scaling parameter. c_i is the maximum distance to the neighbouring nodes. Two-dimensional shape functions require 2D weight functions, and here we use the tensor product of one-dimensional forms [7, 10] with a square nodal domain of influence. The size of the influence domain is d_{mk}, where $k=x,y$ in the x and y directions respectively. The weight function of a node i at point $\mathbf{x}$ is then written as

$$w\left(\mathbf{x}-\mathbf{x}_i\right)=w_{1D}\left(r_x\right)\cdot w_{1D}\left(r_y\right)=w_x\cdot w_y \tag{18}$$

where $r_k=\frac{\|k-k_i\|}{d_{mk}}$ and $d_{mk}=d_{max}\cdot c_{ki}$ and c_{ki} is calculated as

$$c_i=\max_{j\in S_j}\left\|\mathbf{x}-\mathbf{x}_i\right\|. \tag{19}$$

S_j is a set of surrounding nodes, found here using the information from the Voronoi diagram of the nodal distribution [81, 82]

$$S_j=\left[j:V\left(j\right)\cap V\left(i\right)\neq\varnothing\right] \tag{20}$$

where $V\left(i\right)$ is the Voronoi cell of node i. For illustrative purposes a sample 2D grid of nodes is shown in Figure 1(a), its Voronoi diagram is shown in Figure 1(b) and the corresponding rectangular nodal domains of influence (reduced in size for clarity) are shown in Figure 1(c).

Integration of the weak form to provide the discretized algebraic equations in Equation 5 is carried out here using Gauss quadrature in the EFGM. To facilitate this, in this study we use structured grids of nodes which also delineate the quadrature cells. As will be shown below, this allows for a straightforward refinement algorithm to be used. An alternative to quadrature is nodal integration which is first proposed in [83] for linear elasto-static problems, in order to avoid the cell based integration in EFGM. Instability due to under-integration is treated by adding the square of the residual in the equilibrium equation. Stabilized confirming nodal integration for meshfree Galerkin methods is first described in [84], using strain smoothing as a stabilization as compared to the residual in [83]. Strain smoothing avoids the need to calculate shape function derivatives at node and has been extended to nonlinear problems in [85].

2.2 Finite deformation and elasto-plasticity

There are relatively few changes required to model finite deformation and elasto-plasticity with a meshless approach as opposed to one using finite elements. Here, an updated Lagrangian scheme is used in which

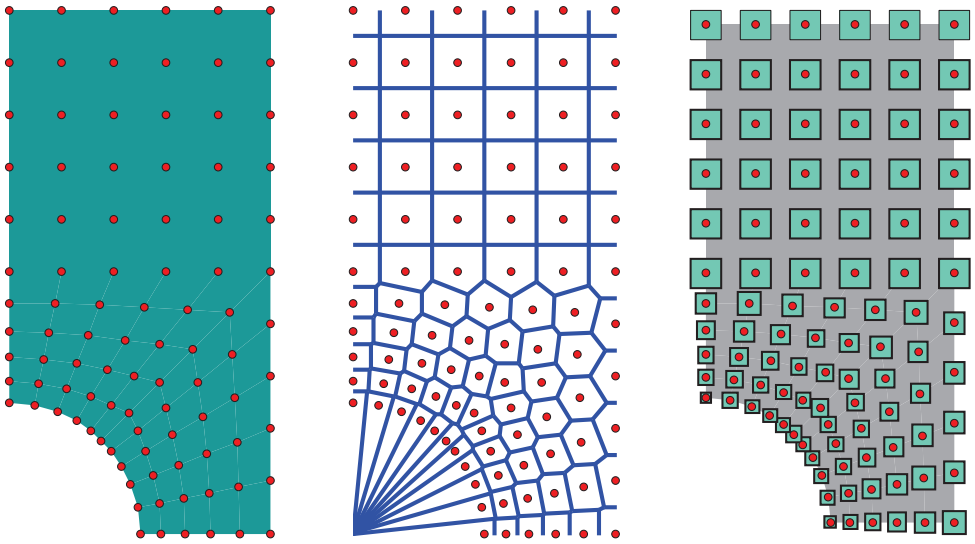

(a) (b) (c)

Figure 1: Problem discretization, Voronoi diagram and corresponding nodal domains of influence

deformation gradient is the fundamental measure of deformation providing the relationship between the current and reference configurations, i.e.

$$\mathbf{F} = \frac{\partial \mathbf{x}}{\partial \mathbf{X}}, \tag{21}$$

where $\mathbf{x}$ and $\mathbf{X}$ are the coordinates of a point in the current and reference configurations respectively. The work-conjugate stress and strain measures used in this paper are logarithmic strain and Kirchhoff stress [86], which are given as [87]

$$\boldsymbol{\varepsilon} = \frac{1}{2} \ln \mathbf{b}, \qquad \boldsymbol{\tau} = J\boldsymbol{\sigma}, \tag{22}$$

where $\mathbf{b}$ is the left Cauchy-Green tensor and J is the determinant of the deformation gradient $\mathbf{F}$. The updated deformation gradient $\mathbf{F}_n$ at the end of increment n is written as

$$\mathbf{F}_n = \Delta\mathbf{F}\ \mathbf{F}_{n-1}, \qquad \Delta\mathbf{F} = \left[\mathbf{I} - \delta\mathbf{F}\right]^{-1}, \qquad \delta\mathbf{F} = \sum_{i=1}^{L} \Delta\mathbf{u}_i \begin{bmatrix} \frac{\partial \phi}{\partial x} \\ \frac{\partial \phi}{\partial y} \end{bmatrix}_i^T, \tag{23}$$

where $\mathbf{F}_{n-1}$ is the value of deformation gradient at the end of previous increment, $\mathbf{I}$ is the unit matrix, L is the number of nodes in support and $\Delta\hat{\mathbf{u}}_i$ is the vector of incremental nodal parameters (or fictitious nodal values). The trial elastic left Cauchy-Green strain tensor is written as

$$\mathbf{b}^e_{tr} = \Delta\mathbf{F} \cdot \mathbf{b}^e_{n-1} \cdot \Delta\mathbf{F}^T, \tag{24}$$

Equation 24 can be used in Equation 22 to calculate the trial elastic strain, which is input to the constitutive model. In this study the Prandtl-Reuss constitutive model is used, which comprises the von-Mises yield

function with perfect plasticity and associated flow. The consistent or algorithmic tangent is used for stress updating, which leads to asymptotic quadratic convergence of the global Newton-Raphson algorithm. Effective plastic strain is used as one of the measures to evaluate the performance of the proposed model and is given as

$$\overline{\varepsilon^p} = \sqrt{\frac{2}{3}\left(\boldsymbol{\varepsilon}^p\right)^T\left(\boldsymbol{\varepsilon}^p\right)}, \tag{25}$$

where $\boldsymbol{\varepsilon}^p = \boldsymbol{\varepsilon}^e_{tr} - \boldsymbol{\varepsilon}^e$ is the plastic logarithmic strain vector, $\boldsymbol{\varepsilon}^e_{tr}$ is the trial elastic logarithmic strain vector and $\boldsymbol{\varepsilon}^e$ is elastic logarithmic strain vector. In this case Equation 6 is written as

$$K_{ij} = \int_{\Omega} \mathbf{G_i^T a G_j d\Omega}, \tag{26}$$

where

$$\mathbf{G}_i = \begin{bmatrix} \frac{\partial \phi_i}{\partial x} & 0 \\ 0 & \frac{\partial \phi_i}{\partial y} \\ \frac{\partial \phi_i}{\partial y} & 0 \\ 0 & \frac{\partial \phi_i}{\partial x} \end{bmatrix}, \tag{27}$$

and $\mathbf{a}$ is the isotropic spatial consistent or algorithmic tangent and is written as

$$\mathbf{a} = \frac{1}{2J}\mathbf{D}^{alg}\mathbf{L}\mathbf{B}^a - \mathbf{S} \tag{28}$$

where

$$\mathbf{L} = \frac{\partial \ln\left(\mathbf{b}^e_{tr}\right)}{\partial \mathbf{b}^e_{tr}}, \qquad \left(\mathbf{B}^a\right)_{ijkl} = \delta_{ik}\left(\mathbf{b}^e_{tr}\right)_{jl} + \delta_{jk}\left(\mathbf{b}^e_{tr}\right)_{il}, \qquad \left(\mathbf{S}\right)_{ijkl} = \left(\boldsymbol{\sigma}\right)_{il}\delta_{jk}. \tag{29}$$

Here $\mathbf{D}^{alg}$ is the small strain consistent or algorithmic tangent, $\mathbf{L}$ is the derivative of the symmetric second-order tensor with respect to its component, the detail of which is given in [88], while $\mathbf{S}$ is known as the non-symmetric stress corrector and δ_{ij} is the Kronecker delta.

2.3 Error estimation and adaptivity in the EFGM

Adaptive refinement algorithms when applied to finite elements work element-by-element. For the EFGM no elements are present so instead we assess error quadrature cell by quadrature cell. Figure 2 shows a flowchart of the overall adaptive algorithm. Three components are required in an adaptive algorithm for nonlinear analysis:

1. estimation of discretization error;
2. refinement strategy;
3. data transfer between the consecutive discretizations.

Each are discussed with reference to the meshless modelling used here in turn below.

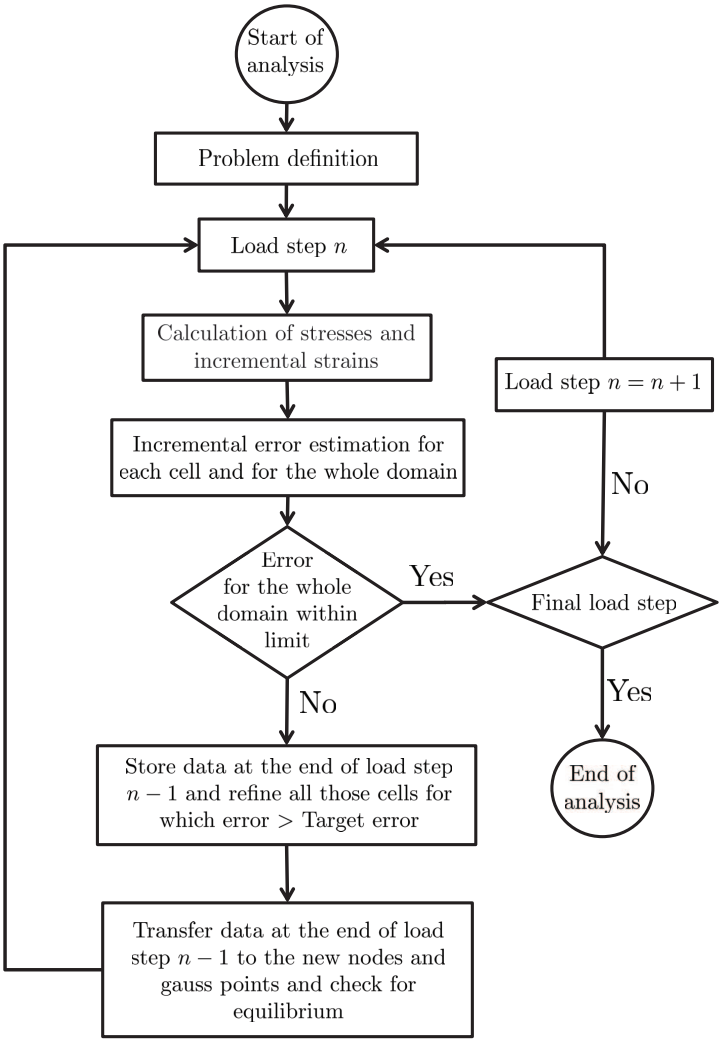

Figure 2: Adaptive algorithm

2.3.1 Error estimation for linear elasto-static problems

Firstly we explain the error estimation procedure for the EFGM due to Chung and Belytschko [70], which is confined to linear elasto-static problems. This procedure is extended to nonlinear problems in the next section.

Recovery type error estimation procedures for FE analysis, based on smoothing procedures applied to stress and strain fields, are not directly applicable to the EFGM, because the derived stress and strain fields are already smooth. Instead, the method introduced in reference [70] estimates the discretization error $\boldsymbol{\sigma}^e$ in the stress field at any point as the difference between the stresses returned at Gauss (i.e. integration) points

in the EFGM and a stress field recovered from the nodal stresses based on reduced domains of influence, i.e.

$$\boldsymbol{\sigma}^e = \boldsymbol{\sigma}^p(\mathbf{x}) - \boldsymbol{\sigma}^h(\mathbf{x}). \tag{30}$$

In the case of the EFGM, the stress vector returned at any point $\mathbf{x}$ is written as

$$\boldsymbol{\sigma}^h(\mathbf{x}) = \sum_{i=1}^{na} \mathbf{D}\mathbf{B}_i \hat{\mathbf{u}}_i \tag{31}$$

where na is the number of nodes in the support of point $\mathbf{x}$ based on the nodal domain of influence d_{ma}. The projected stresses at $\mathbf{x}$ are obtained using

$$\boldsymbol{\sigma}^p(\mathbf{x}) = \sum_{j=1}^{np} \psi_j(\mathbf{x}) \boldsymbol{\sigma}^h(\mathbf{x}_j). \tag{32}$$

Here $\psi_j(\mathbf{x})$ is the shape function of node j at point $(\mathbf{x})$ based on a reduced domain of influence d_{mp} and np is the number of nodes in the support of point $\mathbf{x}$ based on that reduced domain of influence.

Error for the individual cell and for the whole domain can then be found using an appropriate norm. Error in energy norm is used in this paper and is written as

$$\|e\| = \left[\int_\Omega \left| (\boldsymbol{\sigma}^e(\mathbf{x}))^T \mathbf{D}^{-1} (\boldsymbol{\sigma}^e(\mathbf{x})) \right| d\Omega \right]^{\frac{1}{2}}. \tag{33}$$

The relative error in energy norm is often used for adaptive analysis and is written as

$$\eta = \frac{\|e\|}{\|U\|} \times 100, \tag{34}$$

where $\|U\|$ is the energy norm and is written as

$$\|U\| = \left[\int_\Omega \left| \boldsymbol{\sigma}^p(\mathbf{x})^T \mathbf{D}^{-1} \boldsymbol{\sigma}^p(\mathbf{x}) \right| d\Omega \right]^{\frac{1}{2}}. \tag{35}$$

We should here distinguish between the above discretisation-based error estimator, and the model error approach exemplified by the work of Larsson & Runesson [89, 90].

2.3.2 Error estimation in nonlinear problems

For finite element modelling the Zienkiewicz-Zhu (Z^2) error estimator (based on the superconvergent patch recovery method (SPRM)), has been widely used for materially and geometrically nonlinear FE problems. An example can be found in [91] for industrial metal forming problems with elasto-plasticity and finite strains, with estimators based on energy norms, plastic dissipation and rate of plastic work. In [92] the SPRM is used in large deformation problems with hyperelasticity as a material model. An adaptive strategy with error estimation based on an L_2 norm of strain is used in 3D analysis in [93] with large deformation

to model liquefaction phenomena. The Z^2 error estimator is used in the case of viscoplasticity problems, with application to metal forming processes in [94]. In this case the deviatoric stress is used to calculate the error in energy norm due to the incompressible nature of the materials. The work in [94] is further extended in [95] for 3D complex forging simulations and in [96] the SPRM with error based on an L_2 norm in strain is used in analyses involving non-homogeneous soil with large deformation. here we are taking a relatively simple approach by using a recovery-based method, however it should be noted that there is considerable work on more advanced error estimators [60] and of discretization errors due to choice of (pseudo- in this case) time step [97].

Here we extend the use of the recovery type error estimation for EFGM proposed in [70] and as described above, to nonlinear problems modelled with the EFGM including finite deformation and elasto-plasticity. The error in energy norm is used, as first proposed in [98] as a practical error estimator for engineering analysis for linear elasto-static problems. This also follows the approach in [91] also mentioned above. For the nonlinear case the exact incremental error in energy norm for solution step n for the problem domain Ω is equal to [99]

$$\|e\| = \left[\int_{\Omega} \left| \left(\boldsymbol{\tau}_n \left(\mathbf{x} \right) - \boldsymbol{\tau}_n^h \left(\mathbf{x} \right) \right)^T \left(\Delta \boldsymbol{\varepsilon}_n \left(\mathbf{x} \right) - \Delta \boldsymbol{\varepsilon}_n^h \left(\mathbf{x} \right) \right) \right| d\Omega \right]^{\frac{1}{2}}, \tag{36}$$

where $\boldsymbol{\tau}_n \left(\mathbf{x} \right)$ and $\boldsymbol{\tau}_n^h \left(\mathbf{x} \right)$ are the exact and approximate Kirchhoff stresses respectively at point $\mathbf{x}$ for solution step n, while $\Delta \boldsymbol{\varepsilon}_n \left(\mathbf{x} \right)$ and $\Delta \boldsymbol{\varepsilon}_n^h \left(\mathbf{x} \right)$ are the exact and the approximate incremental logarithmic strains at point $\mathbf{x}$ for the solution step n, i.e.

$$\Delta \boldsymbol{\varepsilon}_n \left(\mathbf{x} \right) = \boldsymbol{\varepsilon}_n \left(\mathbf{x} \right) - \boldsymbol{\varepsilon}_{n-1} \left(\mathbf{x} \right), \qquad \Delta \boldsymbol{\varepsilon}_n^h \left(\mathbf{x} \right) = \boldsymbol{\varepsilon}_n^h \left(\mathbf{x} \right) - \boldsymbol{\varepsilon}_{n-1}^h \left(\mathbf{x} \right). \tag{37}$$

For practical engineering problems, exact stresses and strain increments are not available, therefore, as in other recovery methods, projected Kirchhoff stresses $\boldsymbol{\tau}_n^p \left(\mathbf{x} \right)$ and projected incremental logarithmic strains $\Delta \boldsymbol{\varepsilon}_n^p \left(\mathbf{x} \right)$ are used to obtain an error estimator $\|e^p\|$, i.e. replacing the exact quantities in Equation 36.

In the case of the EFGM the projected Kirchhoff stresses and the projected logarithmic strain increment for the solution step n at point $\{x\}$ are determined from the following

$$\boldsymbol{\tau}_n^p \left(\mathbf{x} \right) = \sum_{i=1}^{n} \psi_i \left(\mathbf{x} \right) \boldsymbol{\tau}_n^h \left(\mathbf{x}_i \right), \qquad \Delta \boldsymbol{\varepsilon}_n^p \left(\mathbf{x} \right) = \sum_{i=1}^{n} \psi_i \left(\mathbf{x} \right) \Delta \boldsymbol{\varepsilon}_n^h \left(\mathbf{x}_i \right), \tag{38}$$

where $\psi_i \left(\mathbf{x} \right)$ is the shape function of node i evaluated at point $\mathbf{x}$ with reduced nodal support as compared to the support used to obtain the original approximate solution. The approach is therefore similar to that originally proposed for meshless linear elasto-statics in [70] in obtaining projected values but uses the energy norm as the error measure, in addition to the use of finite deformation stress and strain measures.

The incremental global percentage error for the whole domain is written as

$$\eta = \frac{\|e^p\|}{\|U\|} \times 100, \tag{39}$$

where $\|U\|$ is the incremental energy norm for solution step n

$$\|U\| = \left[\int_{\Omega} \left| \left(\boldsymbol{\tau}_n^p \left(\mathbf{x} \right) \right)^T \left(\Delta \boldsymbol{\varepsilon}_n^p \left(\mathbf{x} \right) \right) \right| d\Omega \right]^{\frac{1}{2}} . \tag{40}$$

Equations 36 and 40 can also be integrated over the each individual integration cell Ω_k instead of the whole problem domain Ω to calculate the incremental error in energy norm and incremental energy norm for each cell. For the whole domain Ω we can write squares of the error and energy norms as

$$\|e^p\|^2 = \sum_{k=1}^{nc} \|e^p\|_k^2 , \qquad \|U\|^2 = \sum_{k=1}^{nc} \|U\|_k^2 , \tag{41}$$

where $\|e^p\|_k$ is the incremental error estimate in energy norm for background cell k and $\|U\|_k$ is the incremental energy norm for background cell k.

2.3.3 Refinement strategy & data transfer

Having devised a means of estimating error we now move to the refinement strategy. The approach is the same as that used in the original Z^2 paper [98], where the target is the reduction of the incremental percentage error at the end of each increment for the whole problem domain below a set value $\overline{\eta}$, i.e.

$$\eta < \overline{\eta}. \tag{42}$$

The goal of the adaptive analysis is to distribute the incremental error at the end of each increment equally into each background cell, so the permissible incremental error in each background cell $\overline{\|e\|}_k$ is written as

$$\overline{\|e\|}_k = \frac{\overline{\eta}}{100} \left(\frac{\|U\|^2}{nc} \right)^{\frac{1}{2}} , \tag{43}$$

where nc is the total number of background cells. Integration cells need to be refined for which $\frac{\|e^p\|_k}{\overline{\|e\|}_k} > 1$.

Given a flag to refine in a particular cell, the step-by-step refinement of the cell is illustrated in Figure 3, as suggested in [75]. It is clear from the figure that in the cells which need refinement, five new nodes are inserted, one on each side and one in the middle of the cell, and then the cell is then further divided into four new cells. A major task in nonlinear adaptive analysis is accurate transfer of path dependent variables between the old and new discretizations. In this study the moving least squares (MLS) approximation is used to transfer data from the old nodes and Gauss points to their new counterparts, a strategy suggested in [75]. The reasons for the choice of MLS rather than max-ent are that the Newton process for determining the Lagrange multipliers for the max-ent formulation becomes poorly convergent when mapping points are close to a boundary and secondly max-ent cannot deal with a new node position which falls outside the original domain, as might commonly occur with finite deformationThe path dependent parameters for the nodes are displacement $\mathbf{u}$, elastic strain, plastic strain and the deformation gradient $\mathbf{F}$. For the Gauss points

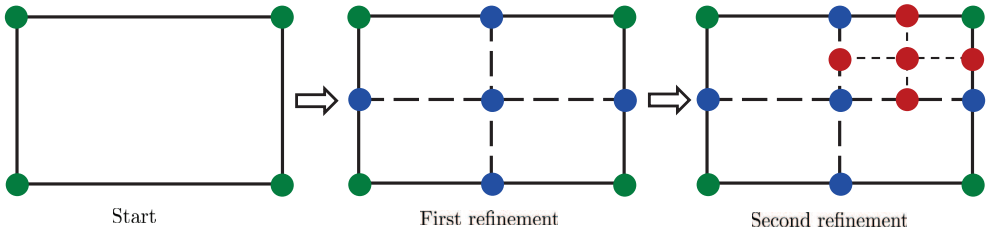

Figure 3: Step by step refinement of the integration cells (the solid filled circles are the nodes defining each cell)

the variables are the same except for the omission of displacement. Writing any of these path dependent variables as ξ, transfer occurs using

$$\xi\left(\mathbf{x}_{new}\right)=\sum_{i=1}^{n_{old}}\psi_i\left(\mathbf{x}_{new}\right)\xi\left(\mathbf{x}_{old}\right)_i, \tag{44}$$

where $\mathbf{x}_{new}$ is the position of the new node or Gauss point, $\mathbf{x}_{old}$ is the position of old nodes or Gauss points, n_{old} is the number of old nodes or Gauss points in the support of $\mathbf{x}_{new}$ and $\psi_j\left(\mathbf{x}_{new}\right)$ are MLS shape functions, the detailed derivation of which can be found in many papers on meshless methods, e.g. [8].

3 NUMERICAL EXAMPLES

Numerical examples are now given to demonstrate the correct implementation and performance of the full meshless modelling approach whose components have been described above. All are taken from or are closely related to problems presented in other publications using finite element analysis. We begin with a simple small deformation problem in 2D to demonstrate the robustness of the basic code, before moving on to examples which demonstrate the full features of the modelling.

3.1 Strip footing collapse

The same problem is also analyzed in [100] to determine a limiting load with finite element analysis. The geometry of the problem, with boundary conditions and material properties are given in Figure 4. The analytical solution for the same problems is also given in [100] as

$$P_{lim}=\left(2+\pi\right)c\approx 5.14c\approx 2.97\sigma_y. \tag{45}$$

where c is the cohesion or shear strength (and for von Mises plasticity $c=\sigma_y/\sqrt{3}$). Only one half of the model is analyzed due to symmetry with plane strain conditions and displacement control. In this case 0.002 m of vertical displacement is applied to the footing in 10 equal steps, which is clearly a small strain problem.

This problem is solved with adaptive analysis with a target error of 20% and the evaluation of adaptive discretizations are shown in Figure 5(a), 5(b), 5(c) and 5(d) with the number of nodes in the consecutive discretizations being 121, 191, 305 and 543 respectively. Contour plots of the effective plastic strain are shown in 6(a). The same problem is also solved with an initial discretization without adaptivity and the contours of effective plastic strain is given in 6(b) for comparison, which clearly shows the effectiveness of the adaptive analysis. The normalized pressure vs displacement curves are given in Figure 7. The same problem is also solved with different initial adaptive discretizations as well as with very fine discretization without adaptivity for the whole problem domain as shown in Figure 5(e). The convergence of the curve for the adaptive analysis as well as for different adaptive initial discretization without adaptivity to the analytical solution is clear from the plot. The solution of this problem with small deformations and matching to a known analytical solution gives confidence to extend the proposed method to problems involving large strains. As will be obvious from the plot, the adaptive solution as shown has a number of jumps in the curve. The jumps represent points where rediscretization is taking place and mapping has been carried out. The jumps are due to changes in equilibrium state of the domain due to the altered discretisation. They should not be confused with jumps in displacements. These plots show results from successive analysis not a single calculation.

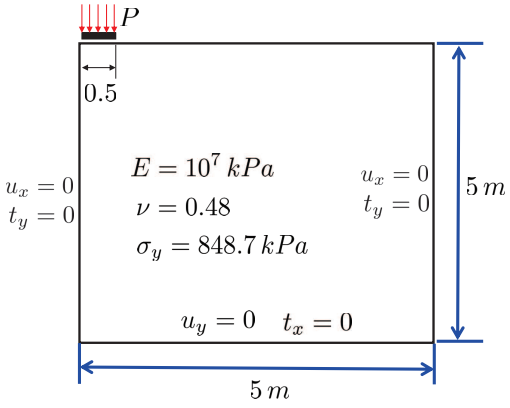

Figure 4: Geometry, boundary conditions and material properties for the strip footing problem

3.2 Perforated tensile specimen

The second problem which begins to challenge the modelling is a perforated thin rectangular plate subject to uniaxial tensile stress applied by prescribed displacements of one set of edges and is used in [99]. The same geometry, boundary conditions and material properties are used here and are as shown in Figure 8. One quarter of the plate is analyzed due to symmetry, using plane stress conditions with displacement control. A total vertical displacement of 0.3 units is applied to the upper horizontal edge of the plate

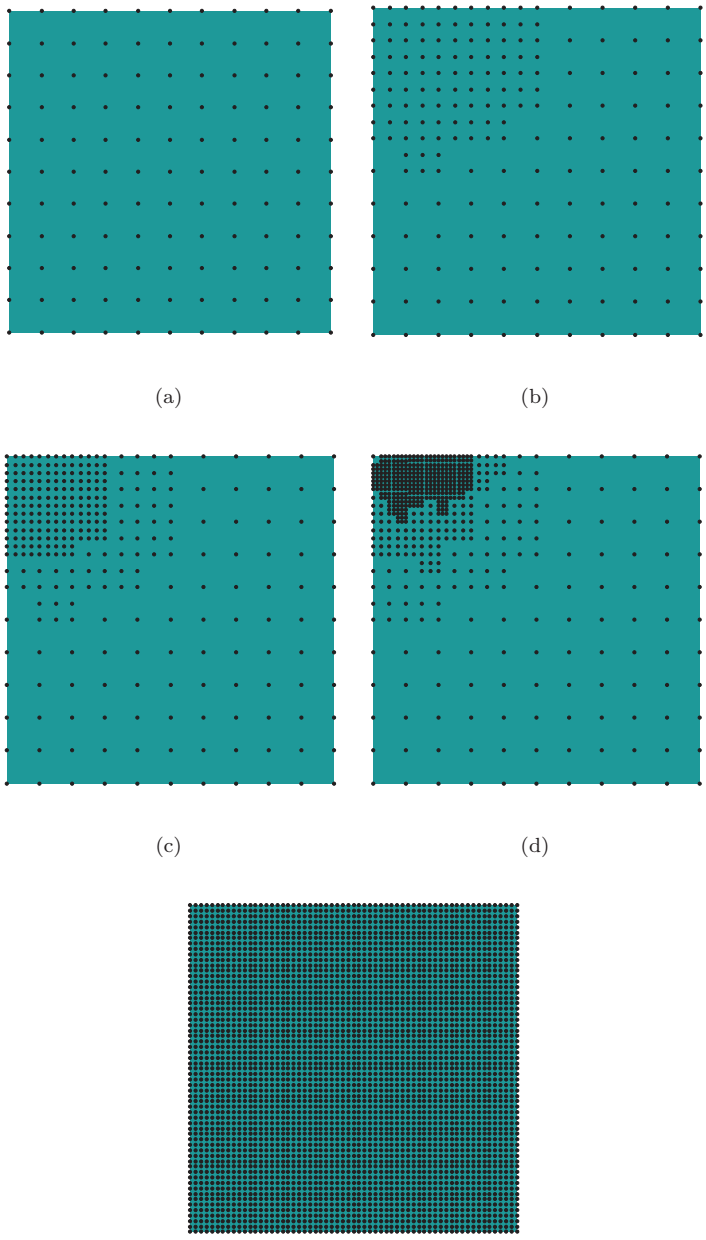

Figure 5: Step by step discretization (a) First (b) Second (c) Third (d) Fourth (e) Reference

over 100 equal steps, clearly making this a finite deformation problem given the original dimensions of the plate. This example is solved using the adaptive procedure with a target error of 18%. During analysis three adaptive refinements are performed. The initial nodal discretization is shown in Figure 9(a), while the first, second and third refinements (at increasing displacements) are given in Figures 9(b) 9(c) and 9(d) respectively. The final deformed configuration (at the final displacement of 0.3 units) is also shown,

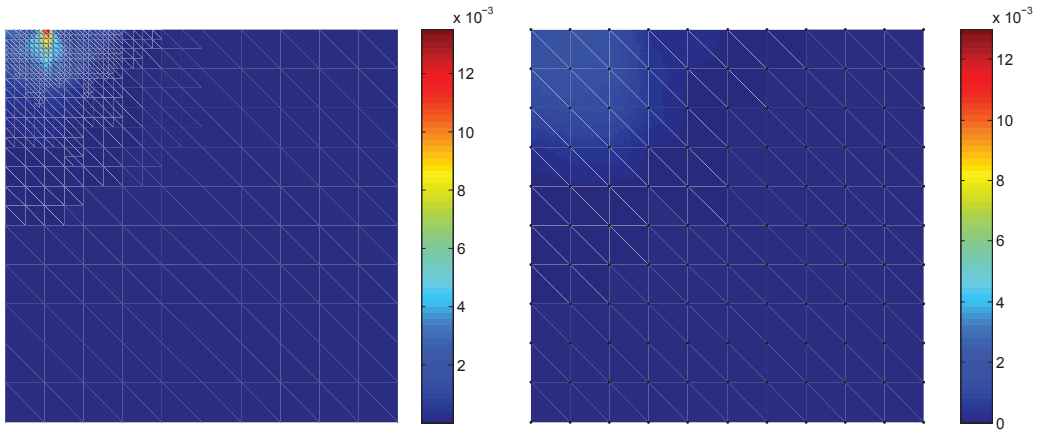

(a) (b)

Figure 6: Effective plastic strain contours over the final deformed configuration for discretizations (a) fine (b) coarse

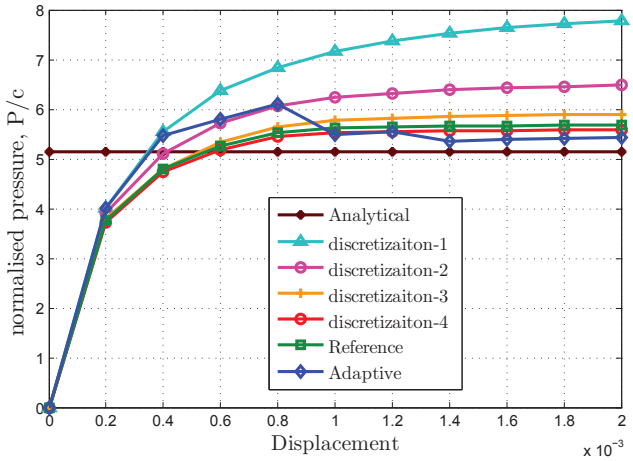

Figure 7: Normalized pressure vs displacement for different discretizations

in Figure 9(e). The numbers of nodes in the consecutive discretizations are 96, 163, 297 and 434. The refinement procedure subdivides integrations cells placing new nodes to define new smaller cells, leading to a roughly structured pattern of refinement. This is clearly unlikely to be the optimal refinement for the load increment as a more unstructured arrangement would be expected to be optimal. However, the simplicity of the refinement algorithm provides a competing advantage. Contours of effective plastic strain over the deformed configuration at the end of the adaptive process is shown in Figure 10(a), in which a developing shear band of finite thickness is clearly evident in the thinning section of the plate adjacent to the hole. The same problem is also solved with an initial coarse discretization without refinement and the contour plot of effective plastic strain at the end of the analysis is shown in Figure 10(b). Comparing these two

figures the sensitivity of the level of refinement of the discretization when conducting finite deformation analysis is clear. Reaction/displacement plots are given in Figure 11, the reaction being the integrated nodal loads along the displaced edge and the displacement the prescribed displacement. Plots are shown for a coarse unrefined analysis against the adaptive analysis and it is clear that the adaptive analysis captures the geometric softening behavior much better than the coarse one. The steps in the adaptive analysis curve occur at points of refinement and are not physically meaningful, although they provide a useful reminder of the adaptive process and follow the presentation in [101]. The effect of re-discretization at refinement is to change the net equilibrium reaction for the given displacement (as one would expect between different refinements in FEA for instance).

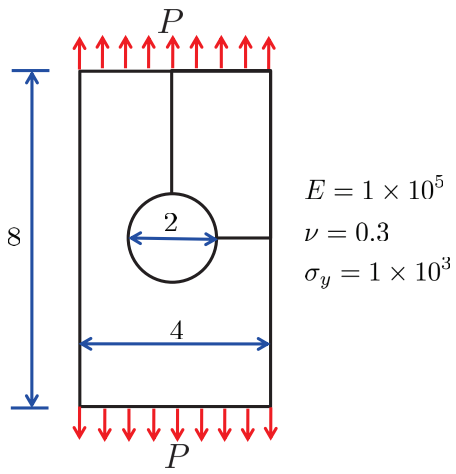

Figure 8: Geometry, boundary conditions and material properties for the perforated tensile specimen (in complementary units)

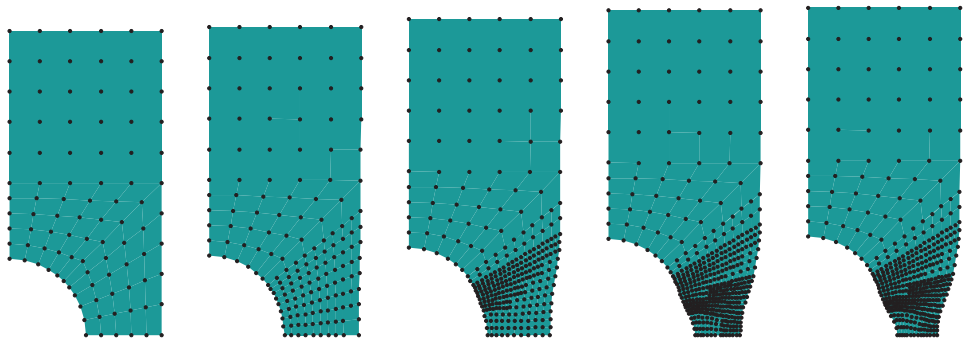

Figure 9: Step by step discretizations: (a) 1st (b) 2nd (c) 3rd (d) 4th (e)Final deformed configurations

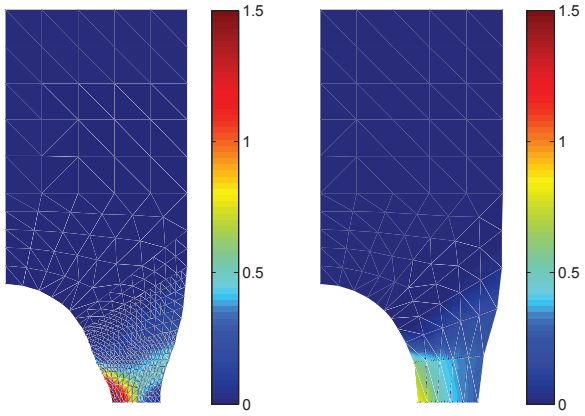

(a) (b)

Figure 10: Effective plastic strain contours over the final deformed configuration for discretizations (a) fine (b) coarse

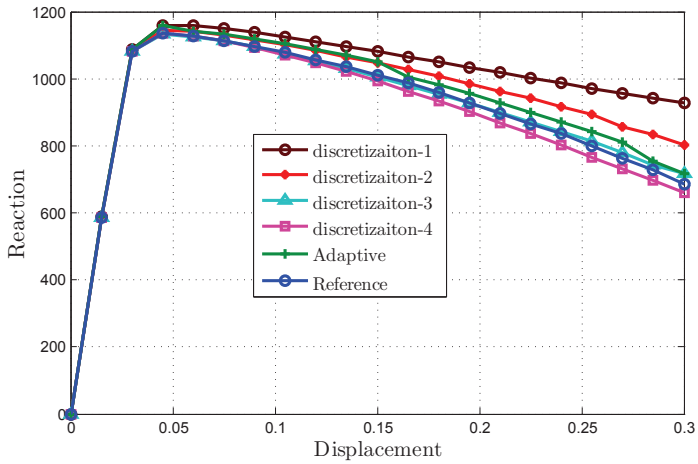

Figure 11: Reaction vs displacement curves for coarse and fine discretizations

3.3 Footing loaded on a vertical cut

The third example comprises the modelling of a block of elasto-plastic material carrying a footing adjacent to a vertical unsupported face. The problem matches that found in a number of references, such as [102–104]. The geometry, material properties and boundary conditions for this problem are given in Figure 12 and it is solved with displacement control under plane strain conditions where a total displacement of 800 mm is applied over 400 equal steps. A rough and rigid footing is used in this case with a Young's modulus 100

times that of the block material. Two refinements are used in this case with a target error of 20%. The initial discretization is shown in Figure 13(a), while the first and second refinements appear in Figures 13(b) & 13(c) respectively. The final deformed configuration for this problem is shown in Figure 13(d). The step by step adaptive procedure concentrates nodes along an emerging shear band as expected and once again the structured nature of the added nodes is clear. The numbers of nodes for the 1st, 2nd and 3rd discretization are 127, 261 and 569 respectively. Contour plots of effective plastic strain over the deformed configuration are shown in Figure 14(a), which clearly shows a shear band of finite thickness. The same problem is also solved with an initial discretization without refinement and the contour plot of effective plastic strain is shown in Figure 14(b). The comparison between the load displacement curves for the adaptive and coarse discretization is shown in Figure 15. Here we can see a perfectly plastic form of failure occurring as the wedge of soil slides as a rigid body along the shear plane. The roughness of the footing and the displacement control serve to control the displacement despite there being near-zero stiffness. It is clear here that the problem requires finite deformation modelling and it is also clear that finite elements along the shear band would be severely distorted.

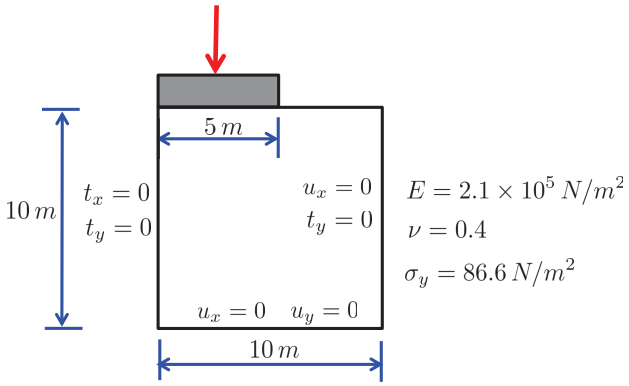

Figure 12: Geometry, boundary conditions and material properties for the footing loaded on a vertical cut problem

3.4 Footing loaded on a slope

The fourth example is another footing, this time on a block of elasto-plastic material resembling a natural slope. This problem also appears in a number of references e.g. [99, 101, 102, 104, 105] and the modelling of problems which are dominated by shear bands are covered using meshless methods in [106–108]. The

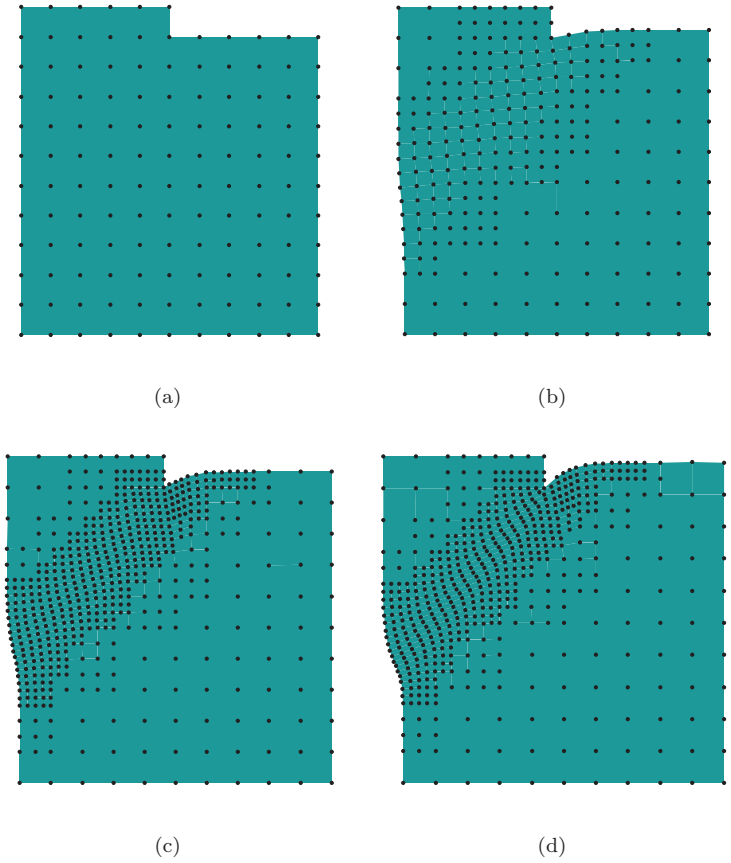

(a) (b)

(c) (d)

Figure 13: Step by step discretization (a) 1st (b) 2nd (c) 3rd (d) Final deformed configurations

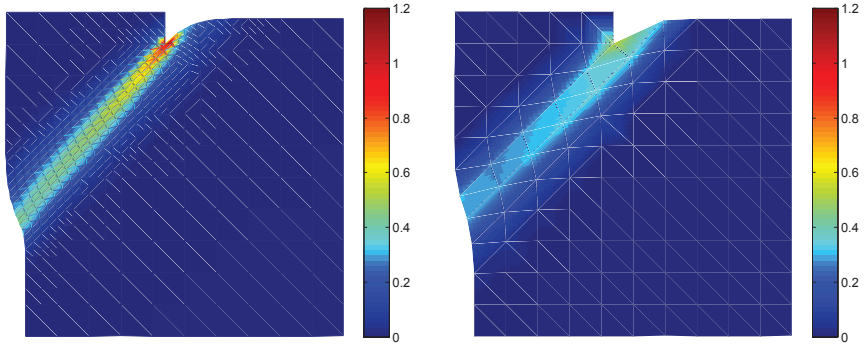

(a) (b)

Figure 14: Effective plastic strain contours over the final deformed configuration for discretizations (a) fine (b) coarse

geometry, material properties and boundary condition for this problem are taken from [99] and all are shown in Figure 16. The problem is solved using displacement control applied to a single point offset from the

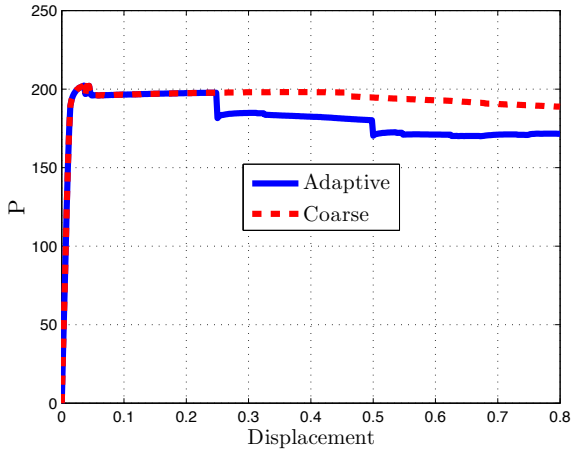

Figure 15: Reaction vs displacement for different discretizations

centre of the footing, under plane strain conditions. A rough and rigid footing is used in this case with a Young's modulus of 100 times that of the slope material. A total displacement of 5.0 units is applied over 100 equal steps. Two adaptive refinements are used in this case with a target error of 10%. The initial discretization is shown in Figure 17(a), while the first and second refinements are given in Figure 17(b), 17(c) with 127, 314 and 668 nodes respectively. The final deformed configuration for this problem is shown in Figure 17(d). The step by step adaptive procedure once again concentrates the nodes along the shear band, which in this case is curved, as would be predicted by simple limit equilibrium theory. The contour plots of the effective plastic strain over the deformed configuration is shown in Figure 18(a), which clearly show a gradually extending shear band of finite thickness. Once again the same problem has been solved with an initial coarse discretization without refinement and the contours of effective plastic strain over the deformed configuration at the end of analysis are shown in Figure 18(b). The load displacement curves for the adaptive and coarse discretization analyses are shown in Figure 19, showing a clear limit load. For the coarse analysis however a small hardening response is evident (for the whole structure, recalling that the elasto-plastic model at the material point is itself only perfectly plastic). For the adaptive case though the response is closer to perfectly plastic.

4 Conclusions

In this paper we have described a new numerical model for use in nonlinear solid mechanics using meshless methods. The model can accommodate both geometrical and material nonlinearity and includes automatic adaptive refinement as well as a number of other innovative features (such as max-ent shape functions). The error estimation procedure proposed by Chung and Belytschko [70] for linear elasto-static problems for the

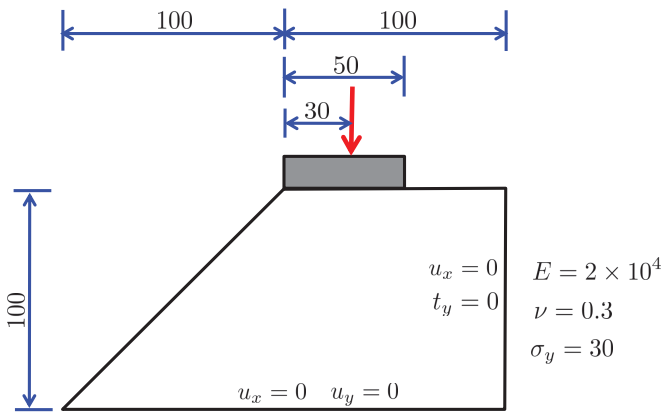

Figure 16: Geometry, boundary conditions and material properties for the footing loaded on a slope problem

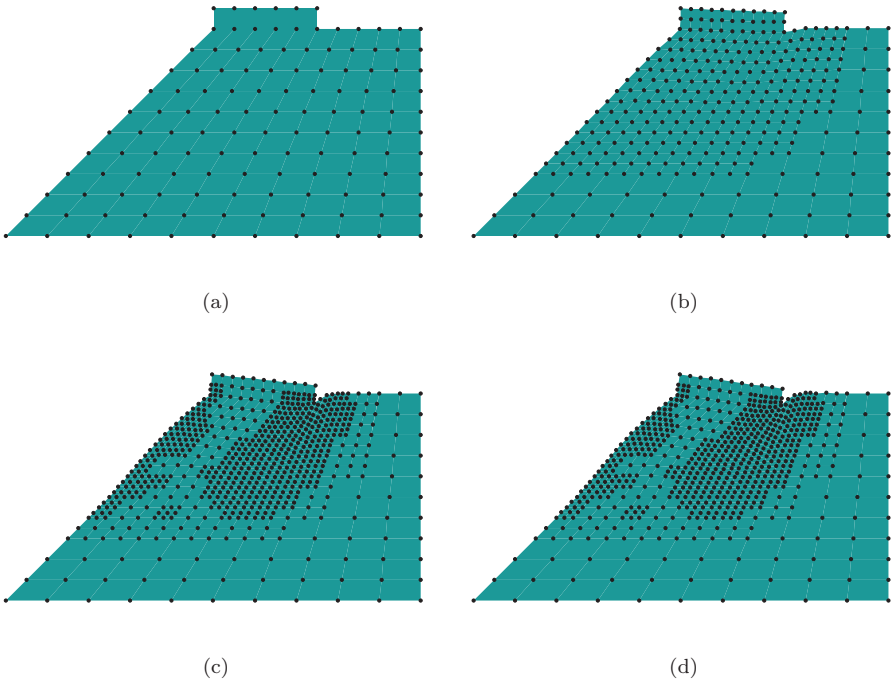

Figure 17: Step by step discretization (a) First (b) Second (c) Third (d) Final deformed configurations

EFGM is extended here to nonlinear problems. An incremental error is calculated for each solution step and is used as the criterion to identify regions for refinement, which can take place very simply both due to the meshless approach and the chosen structured grids of nodes. MLS shape functions are used to transfer the path dependent variables from the old discretization to the new. Three challenging examples have been

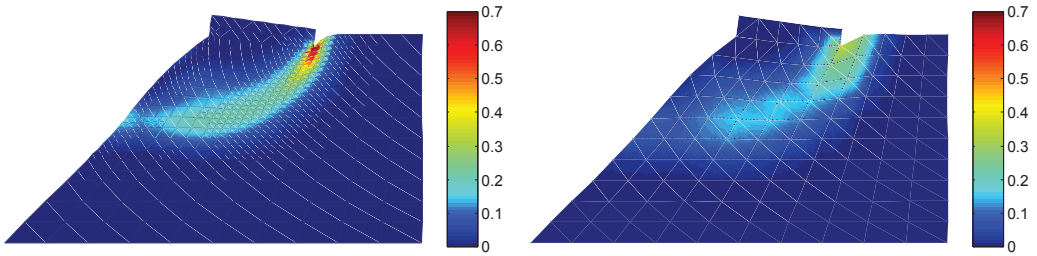

(a) (b)

Figure 18: Effective plastic strain contours over the final deformed configuration for discretizations (a) fine (b) coarse

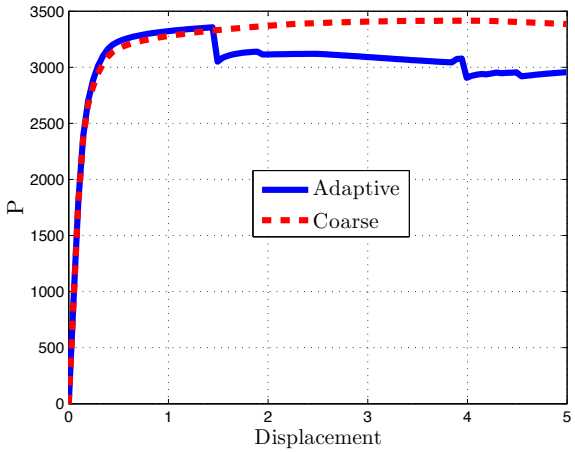

Figure 19: Reaction vs displacement for different discretizations

presented to demonstrate the capabilities of the new modelling procedure as a whole. The model is currently being extended to 3D and performance compared to that of equivalent FE modelling, and these advances will be reported in future papers.

Acknowledgements

The first author is supported by an ORSAS award from Durham University.

References

[1] Liu GR, Gu YT. *An Introduction to Meshfree Methods and their Programming.* Springer, 2005.

[2] Rabczuk T, Zi G, Bordas S, Nguyen-Xuan H. A geometrically non-linear three-dimensional cohesive crack method for reinforced concrete structures. *Engineering Fracture Mechanics* 2008; **75**(16):4740–4758.

[3] Xiao Q, Karihaloo B. Improving the accuracy of XFEM crack tip fields using higher order quadrature and statically admissible stress recovery. *International Journal for Numerical Methods in Engineering* 2006; **66**(9):1378–1410.

[4] Khoei A, Anahid M, Shahim K. An extended arbitrary lagrangian–eulerian finite element method for large deformation of solid mechanics. *Finite Elements in Analysis and Design* 2008; **44**(6):401–416.

[5] Belytschko T, Krongauz Y, Organ D, Fleming M, Krysl P. Meshless methods: An overview and recent developments. *Computer Methods in Applied Mechanics and Engineering* 1996; **139**(1-4):3 – 47.

[6] Fries TP, Matthies HG. Classification and overview of meshfree methods. *Tech. Rep. Informatikbericht-Nr. 2003-03, Institute of Scientific Computing, Technical University Braunschweig* 2004; .

[7] Liu G, Nguyen-Thoi T, Lam K. An edge-based smoothed finite element method (ES-FEM) for static, free and forced vibration analyses of solids. *Journal of Sound and Vibration* 2009; **320**(45):1100 – 1130.

[8] Belytschko T, Lu YY, Gu L. Element-free Galerkin methods. *International Journal for Numerical Methods in Engineering* 1994; **37**:229–256.

[9] Lu YY, Belytschko T, Gu L. A new implementation of the element free Galerkin method. *Computer Methods in Applied Mechanics and Engineering* 1994; **113**(3-4):397 – 414.

[10] Dolbow J, Belytschko T. An introduction to programming the meshless element-free Galerkin method. *Archives of Computational Methods in Engineering* 1998; **5**:207–241.

[11] Belytschko T, Lu YY, Gu L. Crack propagation by element-free Galerkin methods. *Engineering Fracture Mechanics* 1995; **51**(2):295 – 315.

[12] Belytschko T, Tabbara M. Dynamic fracture using element-free Galerkin methods. *International Journal for Numerical Methods in Engineering* 1996; **39**(6):923–938.

[13] Krysl P, Belytschko T. Analysis of thin plates by the element-free Galerkin method. *Computational Mechanics* 1995; **17**:26–35.

[14] Krysl P, Belytschko T. Analysis of thin shells by the element-free Galerkin method. *International Journal of Solids and Structures* 1996; **33**(20-22):3057 – 3080.

[15] Rabczuk T, Areias P, Belytschko T. A meshfree thin shell method for non-linear dynamic fracture. *International journal for numerical methods in engineering* 2007; **72**(5):524–548.

[16] Chen XL, Liu GR, Lim SP. An element free Galerkin method for the free vibration analysis of composite laminates of complicated shape. *Composite Structures* 2003; **59**(2):279 – 289.

[17] Wang Y, Wang Z, Ruan M. Element-free Galerkin method for free vibration of rectangular plates with interior elastic point supports and elastically restrained edges. *Journal of Shanghai University (English Edition)* 2010; **14**:187–195.

[18] Cingoski V, Miyamoto N, Yamashita H. Element-free Galerkin method for electromagnetic field computations. *Magnetics, IEEE Transactions on DOI - 10.1109/20.717759* 1998; **34**(5):3236–3239.

[19] Singh IV, Jain PK. Parallel EFG algorithm for heat transfer problems. *Advances in Engineering Software* 2005; **36**(8):554 – 560.

[20] Singh I. Heat transfer analysis of composite slabs using meshless element free Galerkin method. *Computational Mechanics* 2006; **38**:521–532.

[21] Singh A, Singh IV, Prakash R. Meshless element free Galerkin method for unsteady nonlinear heat transfer problems. *International Journal of Heat and Mass Transfer* 2007; **50**(5-6):1212 – 1219.

[22] Xiong S, Rodrigues J, Martins PAF. Application of the element free Galerkin method to the simulation of plane strain rolling. *European Journal of Mechanics - A/Solids* 2004; **23**(1):77–93.

[23] Yanjin G, Xin W, Guoqun Z, Ping L. A nonlinear numerical analysis for metal-forming process using the rigid-(visco)plastic element-free Galerkin method. *The International Journal of Advanced Manufacturing Technology* May 2009; **42**(1):83–92.

[24] Horton A, Wittek A, Miller K. Towards meshless methods for surgical simulation. *Medical Image Computing and Computer Assisted Intervention (MICCAI) , Copenhagen, Denmark* 2006; :34–42.

[25] Wong KCL, Wang L, Zhang H, Liu H, Shi P. Meshfree implementation of individualized active cardiac dynamics. *Computerized Medical Imaging and Graphics* 2010; **34**(1):91–103.

[26] You W, Liang H, Xing-hua W. Large deformation analysis of pile foundation using meshless method. *World Conference on Earthquake Engineering, Beijing, China* 2008; .

[27] Askes H, de Borst R, Heeres O. Conditions for locking-free elasto-plastic analyses in the Element-Free Galerkin method. *Comput. Method Appl. M* 1999; **173**(1-2):99–109.

[28] Fernández-Méndez S, Huerta A. Imposing essential boundary conditions in mesh-free methods. *Computer Methods in Applied Mechanics and Engineering* 2004; **193**:1257–1275.

[29] Rabczuk T, Belytschko T. Application of particle methods to static fracture of reinforced concrete structures. *International Journal of Fracture* 2006; **137**(1):19–49.

[30] Rabczuk T, Belytschko T. A three-dimensional large deformation meshfree method for arbitrary evolving cracks. *Computer Methods in Applied Mechanics and Engineering* 2007; **196**(29-30):2777–2799.

[31] Rabczuk T, Song J, Belytschko T. Simulations of instability in dynamic fracture by the cracking particles method. *Engineering Fracture Mechanics* 2009; **76**(6):730–741.

[32] Oñate E, Idelsohn S, Zienkiewicz OC, Taylor RL. A finite point method in computational mechanics. applications to convective transport and fluid flow. *International Journal for Numerical Methods in Engineering* 1996; **39**(22):3839–3866.

[33] Onate E, Perazzo F, Miquel J. A finite point method for elasticity problems. *Computers & Structures* 2001; **79**(2225):2151 – 2163.

[34] Liu GR, Dai K, Nguyen T. A smoothed finite element method for mechanics problems. *Computational Mechanics* 2007; **39**:859–877. 10.1007/s00466-006-0075-4.

[35] Liu GR, Nguyen TT, Dai KY, Lam KY. Theoretical aspects of the smoothed finite element method (SFEM). *International Journal for Numerical Methods in Engineering* 2007; **71**(8):902–930.

[36] Dai K, Liu G. Free and forced vibration analysis using the smoothed finite element method (SFEM). *Journal of Sound and Vibration* 2007; **301**(35):803 – 820.

[37] Nguyen-Thoi T, Vu-Do H, Rabczuk T, Nguyen-Xuan H. A node-based smoothed finite element method (NS-FEM) for upper bound solution to visco-elastoplastic analyses of solids using triangular and tetrahedral meshes. *Computer Methods in Applied Mechanics and Engineering* 2010; **199**(4548):3005 – 3027.

[38] Nguyen-Thoi T, Liu GR, Lam KY, Zhang GY. A face-based smoothed finite element method (FS-FEM) for 3d linear and geometrically non-linear solid mechanics problems using 4-node tetrahedral elements. *International Journal for Numerical Methods in Engineering* 2009; **78**(3):324–353.

[39] Nguyen-Xuan H, Bordas S, Nguyen-Dang H. Smooth finite element methods: Convergence, accuracy and properties. *International Journal for Numerical Methods in Engineering* 2008; **74**(2):175–208.

[40] Nguyen-Thoi T, Liu GR, Nguyen-Xuan H, Nguyen-Tran C. Adaptive analysis using the node-based smoothed finite element method (NS-FEM). *International Journal for Numerical Methods in Biomedical Engineering* 2011; **27**(2):198–218.

[41] Sukumar N. Construction of polygonal interpolants: a maximum entropy approach. *International Journal for Numerical Methods in Engineering* 2004; **61**:2159–2181.

[42] Khinchin AI. *Mathematical foundation of information theory*. Dover Publications, Inc. , New York, 1957.

[43] Jaynes ET. Information theory and statistical mechanics-II. *Physical Review* 1957; **108**:171–190.

[44] Jaynes ET. Information theory and statistical mechanics. *Physical Review* 1957; **106**:620–630.

[45] Arroyo M, Ortiz M. Local *maximum-entropy* approximation schemes: a seamless bridge between finite elements and meshfree methods. *International Journal for Numerical Methods in Engineering* 2006; **65**:2167–2202.

[46] Sukumar N, Wright RW. Overview and construction of meshfree basis functions: from moving least squares to entropy approximants. *International Journal for Numerical Methods in Engineering* 2007; **70**:181–205.

[47] Cyron CJ, Arroyo M, Ortiz M. Smooth, second order, non-negative meshfree approximants selected by maximum entropy. *International Journal for Numerical Methods in Engineering* 2009; **79**(13):1605–1632.

[48] Rosolen A, Milln D, Arroyo M. On the optimum support size in meshfree methods: A variational adaptivity approach with maximum-entropy approximants. *International Journal for Numerical Methods in Engineering* 2010; **82**(7):868–895.

[49] González D, Cueto E, Doblaré M. A higher order method based on local maximum entropy approximation. *International Journal for Numerical Methods in Engineering* 2010; **83**(6):741–764.

[50] Ortiz A, Puso M, Sukumar N. Maximum-entropy meshfree method for compressible and near-incompressible elasticity. *Computer Methods in Applied Mechanics and Engineering* 2010; **199**(25-28):1859 – 1871.

[51] Ortiz A, Puso M, Sukumar N. Maximum-entropy meshfree method for incompressible media problems. *Finite Elements in Analysis and Design* 2011; **47**(6):572 – 585.

[52] Millán D, Rosolen A, Arroyo M. Thin shell analysis from scattered points with maximum-entropy approximants. *International Journal for Numerical Methods in Engineering* 2011; **85**(6):723–751.

[53] Kaljević I, Saigal S. An improved element free Galerkin formulation. *International Journal for Numerical Methods in Engineering* 1997; **40**(16):2953–2974.

[54] Chen JS, Wang HP. New boundary condition treatments in meshfree computation of contact problems. *Computer Methods in Applied Mechanics and Engineering* 2000; **187**(34):441 – 468.

[55] Li S, Liu WK. *Meshfree Particle Methods*. Springer, Berlin, 2004.

[56] Ladevèze P, Leguillon D. Error estimate procedure in the finite element method and applications. *SIAM Journal on Numerical Analysis* 1983; **20**(3):485–509.

[57] Ladevèze P, Pelle J, Rougeot P. Error estimation and mesh optimization for classical finite elements. *Engineering Computations* 1991; **8**(3):69–80.

[58] Ladevèze P, Rougeot P. New advances on a posteriori error on constitutive relation in f.e. analysis. *Computer Methods in Applied Mechanics and Engineering* 1997; **150**(14):239 – 249.

[59] Ladevèze P, Moës N, Douchin B. Constitutive relation error estimators for (visco)plastic finite element analysis with softening. *Computer Methods in Applied Mechanics and Engineering* 1999; **176**:247 – 264.

[60] Ladevèze P, Moës N. A new a posteriori error estimation for nonlinear time-dependent finite element analysis. *Computer Methods in Applied Mechanics and Engineering* 1998; **157**(12):45 – 68.

[61] Ladevèze P, Moës N. A posteriori constitutive relation error estimators for nonlinear finite element analysis and adaptive control. *Advances in Adaptive Computational Methods in Mechanics*, *Studies in Applied Mechanics*, vol. 47, Ladev̀(e)ze P, Oden J (eds.). Elsevier, 1998; 231 – 256.

[62] Ladevèze P. Constitutive relation errors for f.e. analysis considering (visco-) plasticity and damage. *International Journal for Numerical Methods in Engineering* 2001; **52**(5-6):527–542.

[63] Babuška I, Rheinboldt WC. A-posteriori error estimates for the finite element method. *International Journal for Numerical Methods in Engineering* 1978; **12**(10):1597–1615.

[64] Kelly DW, De S R Gago JP, Zienkiewicz OC, Babuška I. A posteriori error analysis and adaptive processes in the finite element method: Part I-error analysis. *International Journal for Numerical Methods in Engineering* 1983; **19**(11):1593–1619.

[65] Mark Ainsworth JTO. *A Posteriori Error Estimation in Finite Element Analysis*. John Wiley & Sons, NewYork, 2000.

[66] Babuška I, Strouboulis T, Upadhyay C. A model study of the quality of a posteriori error estimators for linear elliptic problems. error estimation in the interior of patchwise uniform grids of triangles. *Computer Methods in Applied Mechanics and Engineering* 1994; **114**(34):307 – 378.

[67] Babuška I, Strouboulis T, Upadhyay CS. A model study of the quality of a posteriori error estimators for finite element solutions of linear elliptic problems, with particular reference to the behavior near the boundary. *International Journal for Numerical Methods in Engineering* 1997; **40**(14):2521–2577.

[68] Babuška I, Strouboulis T, Upadhyay CS, Gangaraj SK, Copps K. Validation of a posteriori error estimators by numerical approach. *International Journal for Numerical Methods in Engineering* 1994; **37**(7):1073–1123.

[69] Larsson F, Hansbo P, Runesson K. Strategies for computing goal-oriented a posteriori error measures in non-linear elasticity. *International Journal for Numerical Methods in Engineering* 2002; **55**(8):879–894.

[70] Chung HJ, Belytschko T. An error estimate in the EFG method. *Computational Mechanics* 1998; **21**:91–100.

[71] Hussler-Combe U, Korn C. An adaptive approach with the element-free-Galerkin method. *Computer Methods in Applied Mechanics and Engineering* 1998; **162**(1-4):203 – 222.

[72] Gavete L, Falcn S, Ruiz A. An error indicator for the element free Galerkin method. *European Journal of Mechanics - A/Solids* 2001; **20**(2):327 – 341.

[73] Gavete L, Cuesta JL, Ruiz A. A numerical comparison of two different approximations of the error in a meshless method. *European Journal of Mechanics - A/Solids* 2002; **21**(6):1037 – 1054.

[74] Gavete L, Cuesta JL, Ruiz A. A procedure for approximation of the error in the EFG method. *International Journal for Numerical Methods in Engineering* 2002; **53**(3):677–690.

[75] Rabczuk T, Belytschko T. Adaptivity for structured meshfree particle methods in 2D and 3D. *International Journal for Numerical Methods in Engineering* 2005; **63**(11):1559–1582.

[76] Luo Y, Häussler-Combe U. A gradient-based adaptation procedure and its implementation in the element-free Galerkin method. *International Journal for Numerical Methods in Engineering* 2003; **56**(9):1335–1354.

[77] Liu GR, Tu ZH. An adaptive procedure based on background cells for meshless methods. *Computer Methods in Applied Mechanics and Engineering* 2002; **191**(17-18):1923 – 1943.

[78] Lee GH, Chung HJ, Choi CK. Adaptive crack propagation analysis with the element-free Galerkin method. *International Journal for Numerical Methods in Engineering* 2003; **56**(3):331–350.

[79] Lee CK, Zhou CE. On error estimation and adaptive refinement for element free Galerkin method: Part I: stress recovery and a posteriori error estimation. *Computers & Structures* 2004; **82**(4-5):413 – 428.

[80] Lee CK, Zhou CE. On error estimation and adaptive refinement for element free Galerkin method: Part II: adaptive refinement. *Computers & Structures* 2004; **82**(4-5):429 – 443.

[81] Le CV, Askes H, Gilbert M. Adaptive element-free Galerkin method applied to the limit analysis of plates. *Computer Methods in Applied Mechanics and Engineering* 2010; **199**(37-40):2487 – 2496.

[82] Le CV. Novel numerical procedures for limit analysis of structures - meshfree methods and mathematical programming. PhD Thesis, University of Sheffield 2010.

[83] Beissel S, Belytschko T. Nodal integration of the element-free Galerkin method. *Computer Methods in Applied Mechanics and Engineering* 1996; **139**(14):49 – 74.

[84] Chen JS, Wu CT, Yoon S, You Y. A stabilized conforming nodal integration for Galerkin mesh-free methods. *International Journal for Numerical Methods in Engineering* 2001; **50**(2):435–466.

[85] Chen JS, Yoon S, Wu CT. Non-linear version of stabilized conforming nodal integration for Galerkin mesh-free methods. *International Journal for Numerical Methods in Engineering* 2002; **53**(12):2587–2615.

[86] Ji W, Waas AM, Bazant ZP. Errors caused by non-work-conjugate stress and strain measures and necessary corrections in finite element programs. *Journal of Applied Mechanics* 2010; **77**(4):044504.

[87] Coombs WM, Crouch RS, Augarde CE. 70-line 3D finite deformation elastoplastic finite-element code. *Proc. Numerical Methods in Geotechnical Engineering (NUMGE), Trondheim, Norway*, June 3-5 2010; 151–156.

[88] Miehe C. Comparison of two algorithms for the computation of fourth-order isotropic tensor functions. *Computers and Structures* 1998; **66**(1):37 – 43.

[89] Larsson F, Runesson K. Modeling and discretization errors in hyperelasto-(visco-)plasticity with a view to hierarchical modeling. *Computer Methods in Applied Mechanics and Engineering* 2004; **193**(4851):5283 – 5300. ¡ce:title¿Advances in Computational Plasticity¡/ce:title¿.

[90] Johansson H, Runesson K, Larsson F. Calibration of a class of non-linear viscoelasticity models with adaptive error control. *Computational Mechanics* 2007; **41**:107–119. 10.1007/s00466-007-0172-z.

[91] Peric D, Vaz M, Jr, Owen D. On adaptive strategies for large deformations of elasto-plastic solids at finite strains: computational issues and industrial applications. *Computer Methods in Applied Mechanics and Engineering* 1999; **176**(1-4):279 – 312.

[92] Hai G, Hisashi N. A study of applying the superconvergent patch recovery (SPR) method to large deformation problem. *Journal of the Society of Naval Architects of Japan* 2000; (187):201–208.

[93] Xiaowei T, Tadanobu S. Adaptive mesh refinement and error estimate for 3-D seismic analysis of liquefiable soil considering large deformation. *Journal of natural disaster science* 2004; **26**(1):37–48.

[94] L Fourment JC. Error estimators for viscoplastic materials: application to forming processes. *Engineering Computations* 1995; **12**:469 – 490.

[95] Boussetta R, Coupez T, Fourment L. Adaptive remeshing based on a posteriori error estimation for forging simulation. *Computer Methods in Applied Mechanics and Engineering* 2006; **195**(48-49):6626 – 6645.

[96] Hu Y, Randolph MF. H-adaptive FE analysis of elasto-plastic non-homogeneous soil with large deformation. *Computers and Geotechnics* 1998; **23**(1-2):61 – 83.

[97] Allix O, Kerfriden P, Gosselet P. On the control of the load increments for a proper description of multiple delamination in a domain decomposition framework. *International Journal for Numerical Methods in Engineering* 2010; **83**(11):1518–1540.

[98] Zienkiewicz OC, Zhu JZ. A simple error estimator and adaptive procedure for practical engineerng analysis. *International Journal for Numerical Methods in Engineering* 1987; **24**:337–357.

[99] Boroomand B, Zienkiewicz O. Recovery procedures in error estimation and adaptivity. Part II: Adaptivity in nonlinear problems of elasto-plasticity behaviour. *Computer Methods in Applied Mechanics and Engineering* 1999; **176**(1-4):127 – 146.

[100] de Souza Neto E, Perić D, Owen D. *Computational Methods for Plasticity: Theory and Applications*. John Wiley and Sons, 2008.

[101] Lu H. Progressive adaptivity formulation in Galerkin meshfree method. PhD Thesis, The University of Iowa, United States – Iowa 2001.

[102] Khoei AR, Tabarraie AR, Gharehbaghi SA. H-adaptive mesh refinement for shear band localization in elasto-plasticity cosserat continuum. *Communications in Nonlinear Science and Numerical Simulation* 2005; **10**(3):253 – 286.

[103] Khoei A, Bakhshiani A. A hypoelasto-viscoplastic endochronic model for numerical simulation of shear band localization. *Finite Elements in Analysis and Design* 2005; **41**(14):1384 – 1400.

[104] Khoei A, Gharehbaghi S, Tabarraie A, Riahi A. Error estimation, adaptivity and data transfer in enriched plasticity continua to analysis of shear band localization. *Applied Mathematical Modelling* 2007; **31**(6):983 – 1000.

[105] Peric D, Hochard C, Dutko M, Owen DRJ. Transfer operators for evolving meshes in small strain elasto-placticity. *Computer Methods in Applied Mechanics and Engineering* 1996; **137**(3-4):331 – 344.

[106] Rabczuk T, Samaniego E. Discontinuous modelling of shear bands using adaptive meshfree methods. *Computer Methods in Applied Mechanics and Engineering* 2008; **197**(6-8):641–658.

[107] Rabczuk T, Areias P. A new approach for modelling slip lines in geological materials with cohesive models. *International Journal for Numerical and Analytical Methods in Geomechanics* 2006; **30**(11):1159–1172.

[108] Rabczuk T, Areias PMA, Belytschko T. A simplified mesh-free method for shear bands with cohesive surfaces. *International Journal for Numerical Methods in Engineering* 2007; **69**(5):993–1021.